

Magnetothermal transport in ultraclean single crystals of Kitaev magnet α -RuCl₃

Y. Xing¹, R. Namba², K. Imamura², K. Ishihara², S. Suetsugu³, T.

Asaba³, K. Hashimoto², T. Shibauchi², Y. Matsuda³, and Y. Kasahara^{4*}

¹College of New Energy and Materials, China University of Petroleum, Beijing 102249, People's Republic of China

²Department of Advanced Materials Science, University of Tokyo, Chiba 277-8561, Japan

³Department of Physics, Kyoto University, Kyoto 606-8502, Japan and

⁴Department of Physics, Kyushu University, Fukuoka 819-0395, Japan

(Dated: October 25, 2024)

The layered honeycomb magnet α -RuCl₃ has emerged as a promising candidate for realizing a Kitaev quantum spin liquid. Previous studies have reported oscillation-like anomalies in the longitudinal thermal conductivity and half-integer quantized thermal Hall conductivity above the antiferromagnetic critical field H_c , generating significant interest. However, the origins of these phenomena remain contentious due to strong sample dependence. Here we re-examine the magnetothermal transport properties using recently available ultra-pure α -RuCl₃ single crystals to further elucidate potential signatures of the spin liquid state. Our findings reveal that while anomalies in thermal conductivity above H_c persist even in ultraclean crystals, their magnitude is significantly attenuated, contrary to the quantum oscillations hypothesis. This suggests that the anomalies are likely attributable to localized stacking faults inadvertently introduced during magnetothermal transport measurements. The thermal Hall conductivity exhibits a half-quantized plateau, albeit with a narrower width than previously reported. This observation aligns with theoretical predictions emphasizing the importance of interactions between chiral edge currents and phonons. These results indicate that structural imperfections exert a substantial influence on both the oscillation-like anomalies and quantization effects observed in magnetothermal transport measurements of α -RuCl₃.

Quantum spin liquid (QSL) is an exotic state of matter in which quantum fluctuations prevent conventional long-range magnetic order, and hosts many fascinating phenomena, such as fractionalized excitations and topological orders [1]. The Kitaev model on a two-dimensional (2D) honeycomb lattice is a novel example of an exactly solvable QSL state that exhibits itinerant Majorana fermions and localized Z_2 fluxes (visons) [2]. In magnetic fields, these emergent quasiparticles give rise to non-Abelian anyons, which can be useful for topological quantum computing. Among candidate materials, the layered honeycomb magnet α -RuCl₃ [3] has been intensively studied as one of the most promising candidates [4, 5]. Although a zigzag antiferromagnetic (AFM) order appears below the Néel temperature $T_N \sim 7$ K in zero field, the signatures of spin fractionalization have been reported by various experiments, suggesting that α -RuCl₃ is in proximity to a Kitaev QSL [6–11]. More importantly, the AFM order is suppressed by in-plane magnetic fields, and the field-induced quantum disordered (FIQD) state above $\mu_0 H_c \sim 8$ T is proposed to be a Kitaev QSL state.

In the FIQD state of α -RuCl₃, two remarkable observations have been reported by thermal transport experiments. One is the half-integer quantized thermal Hall (HIQTH) effect, which has been confirmed by several groups [12–15]. The 2D thermal Hall conductance per honeycomb plane κ_{xy}^{2D} shows a quantized plateau behavior as a function of H and is close to half the value of the thermal conductance quantum $K_0 = \frac{\pi^2 k_B^2}{3h} T$. Moreover, a finite thermal Hall conductivity is observed even when the magnetic field is applied parallel to the in-plane ther-

mal current, a phenomenon known as the planar thermal Hall effect. This effect exhibits half-quantization [15]. Notably, the field-angular variation of the HIQTH conductance has the same sign structure as the topological Chern number expected for the Kitaev QSL [15]. These results provide direct evidence for chiral Majorana modes at the sample edge and non-Abelian anyons in the bulk [2]. The half-quantized planar thermal Hall effect in α -RuCl₃ exhibits intriguing temperature-dependent behavior. The quantization is observed in a limited temperature range of 3.5–6.5 K. At lower temperatures, κ_{xy}^{2D} is reduced to values smaller than the quantized thermal conductance is reduced to be smaller than K_0 . This phenomenon has been interpreted in the context of decoupling between chiral Majorana edge modes and phonons [16, 17]. However, the universality of these observations remains contested. Some research groups report no evidence of the plateau or quantization, instead proposing bosonic magnon origins for the thermal Hall effect [19]. On the other hand, recent experimental observations have revealed two significant concurrent phenomena when a magnetic field is applied parallel to the b -axis: a sign reversal in the planar thermal Hall effect and the closing of an energy gap, resulting in the formation of a Dirac cone [20, 21]. This simultaneous manifestation of these distinct and remarkable physical processes provides compelling evidence supporting the hypothesis that Majorana fermions are responsible for the observed thermal Hall effect [20, 21]. The other remarkable observation is the oscillation-like anomalies of the longitudinal thermal conductivity κ [22–28]. These anomalies have been reproduced, but interpretations of their origin remain highly

controversial. Both intrinsic and extrinsic origins have been discussed, such as charge-neutral fermions in a putative QSL state [22], which may be associated with the Kitaev QSL state [28], and a sequence of magnetic phase transitions induced by stacking faults [23–25].

Sample dependence likely accounts for the conflicting results and interpretations of the thermal Hall effect and thermal conductivity measurements. In fact, α -RuCl₃ is known to be highly susceptible to stacking faults that can be introduced during the crystal growth process and sample handling [29]. The half-integer quantized plateau has only been confirmed for samples grown by the Bridgman method, but there is no such report for the samples grown by the chemical vapor transport (CVT) method. Moreover, even for samples grown by the Bridgman method, the HIQTH effect is observed only in samples with higher longitudinal thermal conductivity than a certain threshold value [30]. As for the thermal conductivity oscillations, some groups reported the enhancement of the oscillation amplitude in samples with lower longitudinal thermal conductivity [18, 24], while the others reported the opposite trend [26]. Thus, the situation calls for further thermal transport studies on samples with an extreme cleanliness.

In this paper, we revisit the magnetothermal transport properties of α -RuCl₃ using ultraclean samples that have been recently synthesized [31]. We found that anomalous behavior manifesting as oscillatory-like features is observed in the magnetic field dependence of the thermal conductivity, $\kappa(H)$, above H_c , but their magnitude is significantly suppressed in the ultraclean samples. This contradicts with the hypothesis of quantum oscillations, indicating that the oscillatory features arise from a sequence of magnetic transitions induced by unavoidable stacking faults. The thermal Hall conductivity exhibits a half-quantized plateau, but its width is strongly reduced in our samples with higher T_N and H_c . We discuss these results in terms of disorder and non-Kitaev interactions.

Single crystals of α -RuCl₃ were grown using a two-step crystal growth method combining with the CVT and sublimation processes [31]. The in-plane longitudinal thermal conductivity κ and the thermal Hall conductivity κ_{xy} were measured by the standard steady-state method with a heat current \mathbf{q} applied along the b -axis. For the measurements of κ_{xy} , magnetic fields \mathbf{H} were applied along the a -axis. The details of the structural and physical properties of our samples are described in Ref. [31].

Figure 1 shows the temperature dependence of κ in zero field. Data of Bridgman sample are also plotted for comparison [15]. The thermal conductivity exhibits a sharp kink anomaly at around $T_N = 7.8$ K, which is higher than that of the Bridgman sample ($T_N = 7.4$ K), as previously reported [31]. Here, T_N was determined from the minima in $d\kappa/dT$ (Fig. 1, inset). The peak of $\kappa(T)$ below T_N is more than twice as large as that of the Bridgman sample and is the highest among those reported so far. This

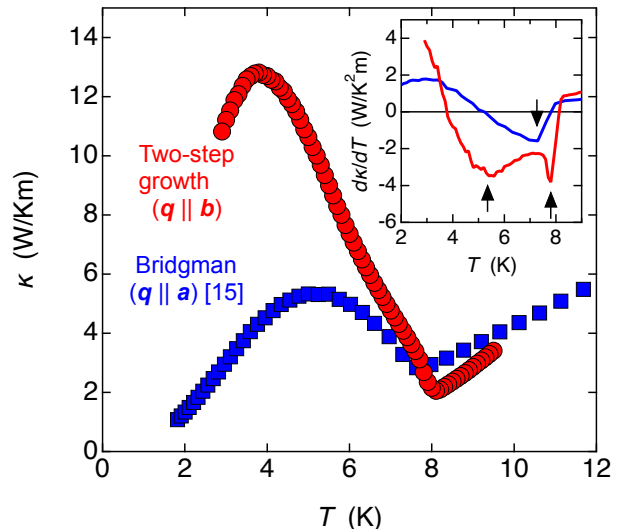


FIG. 1. Temperature dependence of the longitudinal thermal conductivity κ for the ultraclean (two-step sublimation) sample (red) is compared with those of the Bridgman sample (blue) [15]. The heat current \mathbf{q} is applied along the $b(a)$ -axis for the sublimation (Bridgman) samples. The inset shows the temperature dependence of $d\kappa/dT$. The arrows indicates minima in $d\kappa/dT$.

demonstrates the superior quality of the samples with minimal disorder and stacking faults [31]. Hereafter, the two-step sublimation sample will be referred to as the ultraclean sample. Although $\kappa(T)$ of the ultraclean sample looks similar to that of the Bridgman sample, a clear difference can be seen by taking the temperature derivative of $\kappa(T)$, $d\kappa(T)/dT$. Below T_N , two dip structures appear in $d\kappa(T)/dT$ at about 5.5 and 7.8 K, indicating two-step enhancement of κ below T_N , in contrast to a single dip at about 7.4 K for the Bridgman sample (arrows in the inset of Fig. 1). In α -RuCl₃, heat is carried by both magnetic excitations and phonons, $\kappa = \kappa_{\text{mag}} + \kappa_{\text{ph}}$. It has been suggested that κ_{ph} is the dominant contribution, and the peak of κ appears as a result of an enhanced phonon mean free path due to the suppression of spin-phonon scattering upon entering the AFM phase. Since there is no magnetic and structural transition below T_N , the two-step enhancement of $\kappa(T)$ below T_N cannot be explained by phonon contributions alone in the present ultraclean crystal, implying the significant contribution of magnetic excitations. This result, which has never been reported before, suggests the importance of high-quality samples for investigating the intrinsic magnetothermal transport properties of α -RuCl₃.

Figure 2(a) depicts the field dependence of κ for $\mathbf{H} \parallel a$ at 2.5 K in the ultraclean sample. For comparison, the data from samples grown using the Bridgman and CVT methods are also shown [24]. At high magnetic fields above about 8 T, $\kappa(H)$ increases rapidly, and its

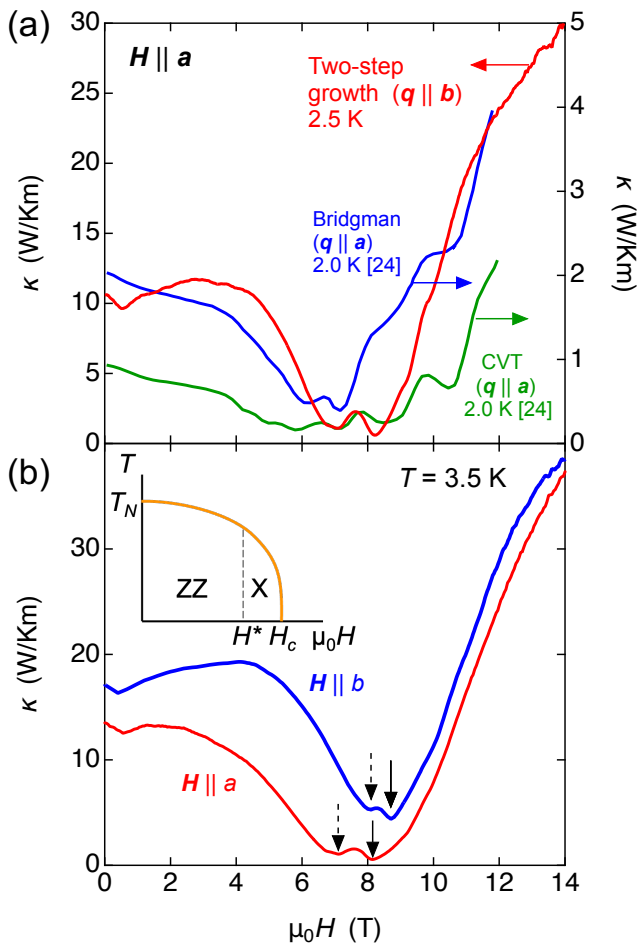


FIG. 2. (a) Field dependence of κ with applied magnetic field along a -axis for ultraclean (two-step sublimation) sample (red) is compared with those of the Bridgman sample (blue) and CVT sample (green) [24]. (b) The H -dependence of κ at 3.5 K for $H \parallel a$ and $H \parallel b$. Sharp minima are caused by the magnetic transitions. The data for $H \parallel b$ are vertically shifted for clarity. The solid (dashed) arrows represent the phase boundary between zigzag (ZZ) magnetic and intermediate X phases at H_c (H^*). The inset shows a schematic phase diagram in in-plane magnetic fields.

magnitude becomes much larger than those of Bridgman and CVT crystals. Remarkably, in the ultraclean sample, despite the significantly higher thermal conductivity in the FIQD state, the oscillatory features are much less prominent compared to the Bridgman and CVT samples. We will discuss this later.

We here discuss the distinctions in the zigzag AFM state between our ultraclean crystal and previously studied Bridgman-grown crystals. Figure 2(b) compares $\kappa(H)$ measured for two orthogonal in-plane field orientations, $H \parallel a$ and $H \parallel b$. As depicted in Fig. 2(b), $\kappa(H)$ exhibits two distinct minima for both field orientations, indicated by dashed and solid arrows. The solid arrow

corresponds to H_c , marking the transition from the AFM phase to the FIQD state. The dashed arrow denotes the transition field H^* from the zigzag AFM phase to the so-called intermediate X phase (Fig. 2(b), inset). It is noteworthy that the anomaly at H^* has not been clearly resolved for $H \parallel b$ in Bridgman-grown samples. This is primarily because H^* in such samples is very close to H_c ($H_c - H^* \lesssim 0.2$ T), making the distinction between these two transitions difficult. The clear separation of H^* and H_c in our ultraclean crystals allows for a more precise characterization of the magnetic phase diagram and the intermediate X phase, which may have significant implications for understanding the magnetic properties of α -RuCl₃.

The oscillation-like anomalies are significantly reduced but still discernible even in our ultraclean crystal. This can be seen clearly by plotting the field derivative of $\kappa(H)$, $[d\kappa/d(\mu_0 H)]/\kappa$, as a function of the normalized field H/H_c in Figs. 3(a) and 3(b). In the FIQD state above H_c , minima are observed for both $H \parallel a$ and $H \parallel b$, as indicated by the arrows. The amplitude of these minima increases with decreasing temperature for $H \parallel a$, consistent with the previously reported oscillation-like anomalies. This indicates that the oscillation-like anomalies above H_c persist even in the ultraclean crystals. However, the fact that significant suppression of the magnitude of anomalies in the ultraclean crystals with higher thermal conductivity obviously contradicts the hypothesis of quantum oscillations. Instead, these anomalies are likely attributed to a series magnetic transitions induced by stacking faults. Although no evidence of stacking faults was detected in the ultraclean samples prior to the experiments, we cannot rule out the possibility that staking faults were introduced during the experiments. In the present thermal conductivity setup, uniaxial stain on crystal is inevitably present [15], which may induce staking faults. These stacking faults could potentially lead to a series of secondary magnetic transition, resulting in oscillation-like anomalies in $\kappa(H)$. The anomalies in $\kappa(H)$ in the FIQD state occur at remarkably similar normalized field values (H/H_c) for both $H \parallel a$ and $H \parallel b$, as indicated by the arrows in Figs. 3(a) and 3(b). This close correspondence in the positions of the anomalies across different field orientations suggests that these anomalies are intrinsically linked to the magnetic anisotropy of α -RuCl₃. It should be noted that even a series of secondary magnetic phases have been reported to exhibit magnetic anisotropy similar to that of the zigzag AFM phase [24]. While further precise measurements on ultraclean crystals are necessary to definitively determine the origin of the oscillatory-like anomalies, the present results suggest an extrinsic origin for these features. The observed suppression of anomaly magnitude in higher-conductivity samples, coupled with the consistent occurrence at similar normalized field values across different field orientations, points towards structural im-

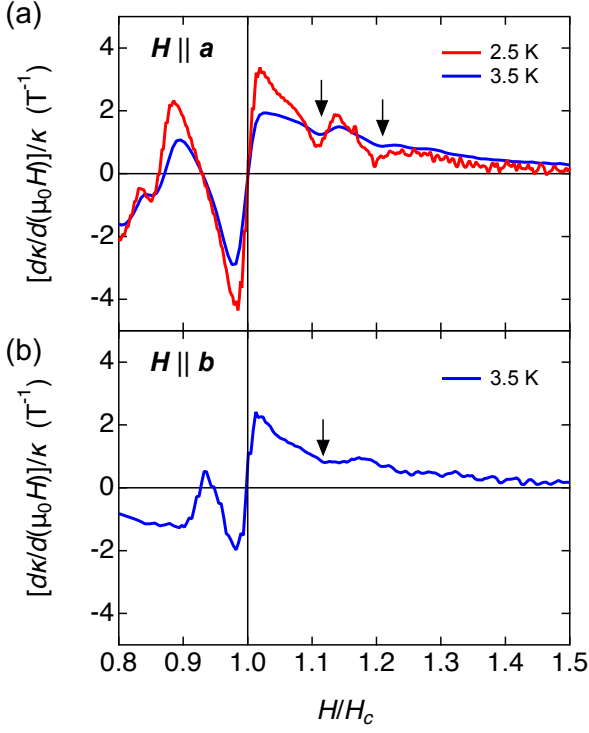


FIG. 3. The normalized field derivative of κ , $[d\kappa/d(\mu_0 H)]/\kappa$, plotted as a function of the normalized field H/H_c for field applied along (a) a - and (b) b -axes ($H_c = 8.2$ T and 8.7 T for a - and b -axes, respectively). The arrows represent the locations of the minima in $[d\kappa/d(\mu_0 H)]/\kappa$. The arrows indicate the well-defined minima in the FIQD state, which likely originate from the oscillation-like features of $\kappa(H)$ reported in the Bridgman and CVT samples.

perfections such as local stacking faults as a probable cause.

Next, we present the results of the thermal Hall effect on the ultraclean sample. Figure 4 depicts the thermal Hall conductivity κ_{xy} with $\mathbf{H} \parallel -a$ at 5.0 K. The dashed violet line represents the HIQTH conductance, $\kappa_{xy}^{2D}/T = \frac{1}{2}(K_0/T)$, where $\kappa_{xy}^{2D} = \kappa_{xy}d$ with the interlayer distance d . Similar to the previous reports, κ_{xy} of the ultraclean sample exhibits a plateau behavior as a function of H , and its value is very close to the HIQTH conductance [12–15]. We note that this represents the first observation of the HIQTH effect with $\mathbf{q} \parallel b$, whereas all previous reports [12–15] utilized $\mathbf{q} \parallel a$.

In previous determinations of the magnitude of κ_{xy} , it was implicitly assumed that $\kappa(\mathbf{q} \parallel a) = \kappa(\mathbf{q} \parallel b)$. However, this equivalence is not necessarily guaranteed by the crystal symmetry [32]. Our present results demonstrate that $\kappa(\mathbf{q} \parallel a)$ is indeed very close to $\kappa(\mathbf{q} \parallel b)$. This result is supported by the data shown in Fig. 1, where $\kappa(\mathbf{q} \parallel b)$ for the ultraclean sample is comparable to $\kappa(\mathbf{q} \parallel a)$ for the Bridgman sample above T_N . The near sample-independence of κ 's magnitude above T_N is

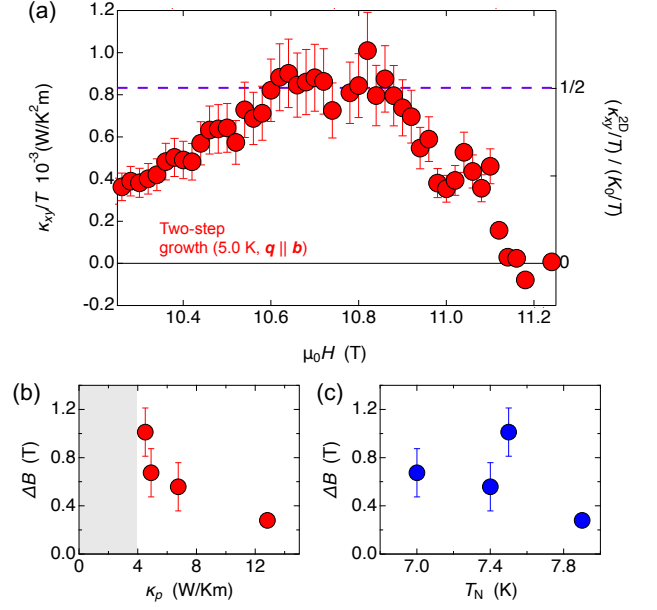


FIG. 4. (a) Field dependence of κ_{xy}/T in the in-plane fields parallel to the a -axis for ultraclean (two-step sublimation) sample at 5.0 K. In the right axis, thermal Hall conductance is shown in units of the quantum thermal conductance $K_0 = (\pi^2/3)(k_B^2/h)/T$. The dashed violet line indicates the half-integer quantization. (b,c) The width of plateau field ΔB at 5.0 K vs (b) thermal conductivity peak κ_p and (c) T_N for the ultraclean sample and the Bridgman samples (Ref. [30]). Samples in the grey region do not exhibit the HIQTH effect.

expected due to significant phonon scattering from paramagnetic fluctuations [33]. Thus, while measurements with $\mathbf{q} \parallel a$ and $\mathbf{q} \parallel b$ using the same sample would be ideal for a direct comparison, our results nonetheless provide additional support for the existence of the HIQTH conductance plateau in α - RuCl_3 .

The observed field range for quantization exhibits differences between ultraclean and Bridgman samples. Quantitatively, the plateau field range in the Bridgman sample is approximately 2.5 times greater than that of the ultraclean sample that possesses higher thermal conductivity. We propose that there are two scenarios for this phenomenon. One is the effect of disorder. This phenomenon bears resemblance to the quantum Hall effect, where disorder plays a crucial role in the emergence of quantized plateaus. In quantum Hall systems, the plateau width decreases with diminishing disorder and vanishes in the absence of disorder [34, 35]. While the underlying mechanisms for quantized plateaus differ fundamentally between Kitaev QSLs and 2D electron gases, analogous arguments regarding the narrowing of plateaus in clean samples have also been proposed for Kitaev QSLs [16, 17]. A critical factor in observing quantized thermal Hall plateaus in Kitaev QSLs is the coupling between chiral Majorana edge modes and phonons. Notably, de-

viations from the quantized thermal Hall value occur at low temperatures, where the phonon mean free path approaches the crystal size. In this ballistic phonon regime, decoupling between phonons and edge currents becomes significant. Consequently, disorder-induced reduction of the phonon mean free path enhances phonon-edge coupling, leading to an expected increase in the plateau field range for samples with higher disorder. The other scenario is the potential influence of non-Kitaev interactions on this phenomenon. These interactions are known to determine T_N . Although the quantitative relationship between the non-Kitaev interactions and T_N in real materials needs to be precisely determined, the observation that T_N of the ultraclean crystal (7.8 K) exceeds that of Bridgman crystals (7.4 K), as illustrated in Fig. 1, suggests stronger non-Kitaev interactions in the former. Given that non-Kitaev interactions modulate the properties of Kitaev QSLs—often detrimentally—they likely impact the quantized plateau behavior.

To investigate the two scenarios mentioned earlier, we plotted the plateau width ΔB against two parameters in Figs. 4(b) and 4(c): the thermal conductivity peak value κ_p (which measures the mean free path of heat carriers) and T_N , respectively. These plots include our data alongside those reported in Ref. [30]. Our analysis reveals two key observations. The sample with higher conductivity tends to have smaller ΔB , and ΔB has the maximum value near the threshold value of κ_p for the quantization [30]. On the other hand, ΔB does not show clear correlation with T_N . These findings suggest that the variation in plateau width appears to be primarily determined by a delicate balance between disorder and phonon-edge coupling strength. While further studies using crystals with minimal disorder are necessary to confirm these conclusions, our results provide valuable insights into the quantization phenomenon in α -RuCl₃.

In summary, we conducted measurements of the longitudinal thermal conductivity and thermal Hall conductivity in ultraclean α -RuCl₃ samples, synthesized using a two-step sublimation method. Our findings reveal discrepancies with previously reported results from magnetothermal transport measurements on α -RuCl₃ grown by Bridgman and CVT methods. We observed oscillation-like anomalies in the longitudinal thermal conductivity of our ultraclean samples. However, the magnitude of these anomalies was significantly suppressed compared to crystals grown by other methods. This observation suggests that these anomalies likely stem from extrinsic effects, possibly due to secondary magnetic transitions induced by local stacking faults unintentionally present even in ultraclean samples. This also underscores the importance of careful sample preparation and characterization in the study of this compound. Furthermore, we detected a half-integer quantized thermal Hall conductance plateau in the ultraclean crystal. Interestingly, the width of this half-integer quantized plateau in the ultra-

clean sample is reduced compared to that grown by the Bridgman method. Our comparative analysis of these systems highlights the crucial importance of disorder and related phonon-edge coupling in shaping the characteristics of quantized thermal Hall plateaus in Kitaev QSLs. This study emphasizes the significance of sample quality and growth methods in understanding the intrinsic properties of α -RuCl₃ and their implications for Kitaev QSL physics.

We thank E.-G. Moon and T. Kurumaji for insightful discussions. This work is supported by Grants-in-Aid for Scientific Research (KAKENHI) (Nos. JP23K13060, JP23H00089, JP24H00965, and JP24K21529) and Grants-in-Aid for Scientific Research on Innovative Areas “Quantum Liquid Crystals” (No. JP19H05824) from Japan Society for the Promotion of Science (JSPS), and CREST (JPMJCR19T5) and PRESTO (JPMJPR2354) from Japan Science and Technology Agency (JST).

* kasahara.yuichi.437@m.kyushu-u.ac.jp

- [1] L. Balents, *Nature* **464**, 199-208 (2010).
- [2] A. Kitaev, *Ann. Phys.* **321**, 2-111 (2006).
- [3] K. W. Plumb, J. P. Clancy, L. J. Sandilands, V. V. Shankar, Y. F. Hu, K. S. Burch, H. Y. Kee, and Y. J. Kim, *Phys. Rev. B* **90**, 041112(R) (2014).
- [4] H. Takagi, T. Takayama, G. Jackeli, G. Khaliullin, and S. E. Nagler, *Nat. Rev. Phys.* **1**, 264-280 (2019).
- [5] S. Trebst and C. Hickey, *Phys. Rep.* **950**, 1-37 (2022).
- [6] S.-H. Do, S.-Y. Park, J. Yoshitake, J. Nasu, Y. Motome, Y. S. Kwon, D. T. Adroja, D. J. Voneshen, K. Kim, T.-H. Jang, J.-H. Park, K.-Y. Choi, and S. Ji, *Nat. Phys.* **13**, 1079-1084 (2017).
- [7] S. Widmann, V. Tsurkan, D. A. Prishchenko, V. G. Mazurenko, A. A. Tsirlin, and A. Loidl, *Phys. Rev. B* **99**, 094415 (2019).
- [8] L. J. Sandilands, Y. Tian, K. W. Plumb, Y. J. Kim, and K. S. Burch, *Phys. Rev. Lett.* **114**, 147201 (2015).
- [9] A. Banerjee, C. A. Bridges, J.-Q. Yan, A. A. Aczel, L. Li, M. B. Stone, G. E. Granroth, M. D. Lumsden, Y. Yiu, J. Knolle, S. Bhattacharjee, D. L. Kovrizhin, R. Moessner, D. A. Tennant, D. G. Mandrus, and S. E. Nagler, *Nat. Mater.* **15**, 733-740 (2016).
- [10] A. Banerjee, P. Lampen-Kelley, J. Knolle, C. Balz, A. A. Aczel, B. Winn, Y. Liu, D. Pajerowski, J. Yan, C. A. Bridges, A. T. Savici, B. C. Chakoumakos, M. D. Lumsden, D. A. Tennant, R. Moessner, D. G. Mandrus, and S. E. Nagler, *npj Quant. Meter.* **3**, 8 (2018).
- [11] C. Balz, P. Lampen-Kelley, A. Banerjee, J. Yan, Z. Lu, X. Hu, S. M. Yadav, Y. Takano, Y. Liu, D. A. Tennant, M. D. Lumsden, D. Mandrus, and S. E. Nagler, *Phys. Rev. B* **100**, 060405(R) (2019).
- [12] Y. Kasahara, T. Ohnishi, Y. Mizukami, O. Tanaka, S. Ma, K. Sugii, N. Kurita, H. Tanaka, J. Nasu, Y. Motome, T. Shibauchi, and Y. Matsuda, *Nature* **559**, 227-231 (2018).
- [13] M. Yamashita, J. Gouchi, Y. Uwatoko, N. Kurita, and H. Tanaka, *Phys. Rev. B* **102**, 220404(R) (2020).
- [14] J. A. N. Bruin, R. R. Claus, Y. Matsumoto, N. Kurita, H.

- Tanaka, and H. Takagi, *Nat. Phys.* **18**, 401-405 (2022).
- [15] T. Yokoi, S. Ma, Y. Kasahara, S. Kasahara, T. Shibauchi, N. Kurita, H. Tanaka, J. Nasu, Y. Motome, C. Hickey, S. Trebst, and Y. Matsuda, *Science* **373**, 568-572 (2021).
- [16] Y. Vinkler-Aviv and A. Rosch, *Phys. Rev. X* **8**, 31023 (2018).
- [17] M. Ye, G. B. Halász, L. Savary, and L. Balents, *Phys. Rev. Lett.* **121**, 147201 (2018).
- [18] É. Lefrançois, G. Grissonnanche, J. Baglo, P. Lampen-Kelley, J. Yan, C. Balz, D. Mandrus, S. E. Nagler, S. Kim, Y.-J. Kim, N. Doiron-Leyraud, and L. Taillefer, *Phys. Rev. X* **12**, 021025 (2022).
- [19] P. Czajka, T. Gao, M. Hirshberger, P. Lampen-Kelley, A. Banerjee, N. Quirk, D. G. Mandrus, S. E. Nagler, and N. P. Ong, *Nat. Mater.* **22**, 36-41 (2023).
- [20] O. Tanaka, Y. Mizukami, R. Harasawa, K. Hashimoto, K. Hwang, N. Kurita, H. Tanaka, S. Fujimoto, Y. Matsuda, E.-G. Moon, and T. Shibauchi, *Nat. Phys.* **18**, 429-435 (2022).
- [21] K. Imamura, S. Suetsugu, Y. Mizukami, Y. Yoshida, K. Hashimoto, K. Ohtsuka, Y. Kasahara, N. Kurita, H. Tanaka, P. Noh, E.-G. Moon, Y. Matsuda, and T. Shibauchi, *Sci. Adv.* **10**, eadk3539 (2024).
- [22] P. Czajka, T. Gao, M. Hirshberger, P. Lampen-Kelley, A. Banerjee, J. Yan, D. G. Mandrus, S. E. Nagler, and N. P. Ong, *Nat. Phys.* **17**, 915-919 (2021).
- [23] S. Suetsugu, Y. Ukai, M. Shimomura, M. Kamimura, T. Asaba, Y. Kasahara, N. Kurita, H. Tanaka, T. Shibauchi, J. Nasu, Y. Motome, and Y. Matsuda, *J. Phys. Soc. Jpn.* **91**, 124703 (2022).
- [24] J. A. N. Bruin, R. R. Claus, Y. Matsumoto, J. Nuss, S. Laha, B. V. Lotsch, N. Kurita, H. Tanaka, and H. Takagi, *APL Mater.* **10**, 090703 (2022).
- [25] É. Lefrançois, J. Baglo, Q. Barthélemy, S. Kim, Y.-J. Kim, and L. Taillefer, *Phys. Rev. B* **107**, 064408 (2023).
- [26] H. Zhang, A. F. May, H. Miao, B. C. Sales, D. G. Mandrus, S. E. Nagler, M. A. McGuire, and J. Yan, *Phys. Rev. Mater.* **7**, 114403 (2023).
- [27] H. Zhang, M. A. McGuire, A. F. May, H.-Y. Chao, Q. Zheng, M. Chi, B. C. Sales, D. G. Mandrus, S. Nagler, H. Miao, F. Ye, and J. Yan, *Phys. Rev. Mater.* **8**, 014402 (2024).
- [28] H. Zhang, H. Miao, T. Z. Ward, D. G. Mandrus, S. E. Nagler, M. A. McGuire, and J. Yan, arXiv:2310.03917.
- [29] H. B. Cao, A. Banerjee, J. Q. Yan, C. A. Bridges, M. D. Lumsden, D. G. Mandrus, D. A. Tennant, B. C. Chakoumakos, and S. E. Nagler, *Phys. Rev. B* **93**, 134423 (2016).
- [30] Y. Kasahara, S. Suetsugu, T. Asaba, S. Kasahara, T. Shibauchi, N. Kurita, H. Tanaka, and Y. Matsuda, *Phys. Rev. B* **106**, L060410 (2022).
- [31] R. Namba, K. Imamura, R. Ishioka, K. Ishihara, T. Miyamoto, H. Okamoto, Y. Shimizu, Y. Saito, Y. Agarmani, M. Lang, H. Murayama, Y. Xing, S. Suetsugu, Y. Kasahara, Y. Matsuda, K. Hashimoto, and T. Shibauchi, *Phys. Rev. Materials* **8**, 074404 (2024).
- [32] T. Kurumaji, *Phys. Rev. Res.* **5**, 023138 (2023).
- [33] D. Hirobe, M. Sato, Y. Shiomi, H. Tanaka, and E. Saitoh, *Phys. Rev. B* **95**, 241112(R) (2017).
- [34] B. Huckestein, *Rev. Mod. Phys.* **67**, 357-396 (1995).
- [35] D. Tong., arXiv:1606.06687.